

BeppoSAX and XMM-Newton spectral study of 4U 1735-44

B. Mück¹, S. Piraino^{1,2} and A. Santangelo¹

¹Institute for Astronomy and Astrophysics Tübingen, Kepler Center for Astro and Particle Physics, University of Tübingen, Sand 1, 72076 Tübingen, Germany

²INAF-IASF di Palermo, via Ugo La Malfa 153, 90146 Palermo, Italy
e-mail: benjamin.mueck@uni-tuebingen.de

ABSTRACT

Context. Low-mass X-ray binary systems consist of a neutron star and a main-sequence companion star. The compact object accretes matter via Roche-lobe overflow, which leads to an accretion disk. In addition to a broad-band continuum emission of a thermal component and a Comptonization part, evidence for a broad iron K_{α} line is found in several sources. Some of them show an asymmetric line profile as well, which could originate from relativistic effects.

Aims. To understand the spectral behavior of the system 4U 1735-44, we study the broad-band spectrum and especially the iron line feature between 6.4 and 6.97 keV. The shape of the line allows one to determine the region where the line is produced. Together with the continuum models, a geometrical model of the source can be proposed. Furthermore, the effects of pile-up in the *XMM-Newton* observation are investigated.

Methods. We analyzed data obtained with the X-ray satellites *BeppoSAX* and *XMM-Newton*. The *XMM-Newton* data were analyzed, specifically taking into account pile-up effects. With the help of the data of these two satellites, we performed a detailed spectral study in an energy range from 0.2–24 keV.

Results. During the observations, the source was in the so-called banana state of an atoll source. Fitting the *BeppoSAX* data, we found line features that we were able to model with a reflection model, whereas the continuum was modeled with a combination of a thermal component and a Comptonization part. The analysis of the *XMM-Newton* data gave evidence for a broad but not asymmetric iron line. We found no broadening or asymmetry of the line because of pile-up.

Key words. accretion, accretion disks – Line: profiles – X-rays: binaries – stars: neutron – X-rays: individuals: 4U 1735-44

1. Introduction

Low-mass X-ray binaries (LMXBs, Hasinger & van der Klis 1989) consist of a compact object and a donor companion star with a mass typically not exceeding one solar mass. In these systems, the compact object is, in most cases, a neutron star, that accretes matter from the donor via Roche-lobe overflow. Because of angular momentum conservation, an accretion disk around the neutron star is formed. X-ray emission from LMXBs is complex, and most likely, different components emerge from different regions. Generally, the spectrum is well reproduced by one or two thermal components in combination with a Comptonized component at higher energies (e.g. Piraino et al. 2012). The origin of the different spectral components is still a matter of debate. Currently, two main models are widely used to describe the LMXB spectrum: the eastern model (Mitsuda et al. 1984, 1989) and the western or Birmingham model (Church & Balucinska-Church 1995, 2004).

In addition, if the accretion disk is illuminated by radiation from the neutron star, reflection features might appear in the spectrum. Indeed, several objects of the class show evidence for broad fluorescence iron K_{α} lines as well as for other lines, which could originate from reflection from an accretion disk. Relativistically broadened fluorescence iron lines were first detected in observations of active galactic nuclei (MCG-6-30-15, Tanaka et al. 1995; Fabian et al. 2000, for a review) and in binary systems containing stellar mass black holes (Cyg X-1, Barr et al. 1985). Actual relativistic models for lines, such as the well-known disk-line model (Fabian et al. 1989, implemented in

XSPEC as diskline) were introduced to explain the asymmetry of the line observed in Cygnus X-1. More recently, improvements in detection techniques allowed evidence for an asymmetric shape of the iron K_{α} line also in LMXBs with neutron stars (Piraino et al. 2000) to be found. To date, a relativistic origin of the fluorescence iron line profile has been discussed in more than ten LMXBs (Bhattacharyya & Strohmayer 2007; Cackett et al. 2008, 2010; di Salvo et al. 2009; D’Aì et al. 2010; Iaria et al. 2009; Pandel et al. 2008; Piraino et al. 2012). We have to observe, however, that Ng et al. (2010), analyzing a large sample of sources observed with *XMM-Newton*, have stressed the importance of the correct instrument pile-up treatment to answer the question whether the iron line is relativistically broadened or not. Very recently, Piraino et al. (2012) and Egron et al. (2013) found that the asymmetry is robust against pile-up effects in the analysis of GX 3+1 and 4U 1705-44, respectively, even when pile-up effects are rigorously taken into account. The superposition of different relativistic effects, such as gravitational redshift and relativistic beaming, shapes the line. These effects strongly depend on the radius where the line is formed and the inclination under which the system is seen.

The presence of such a relativistically broadened line is debated for the LMXB 4U 1735-44. The system is located at a distance of 6.5 ± 1.0 kpc (Galloway et al. 2008) and consists of a neutron star and a companion star with a mass of $0.53 \pm 0.44 M_{\odot}$ (Casares et al. 2006). Matter is accreted by the compact object via Roche-lobe overflow from the companion, leading to a flux in the 2–10 keV range of about 4×10^{-9} erg cm⁻² s⁻¹. The orbital period has been measured to be 4.564 ± 0.005 hr by Corbet

Table 1. Summary of the analysed observations

OBSID	Beginning in UT	End in UT
BeppoSax		
2083600200	03/20/2000 17:03:58	03/21/2000 14:21:58
2122400300	08/26/2000 02:59:56	08/27/2000 04:24:45
2122400400	09/25/2000 06:31:21	09/25/2000 16:04:16
2122400410	09/27/2000 12:41:39	09/27/2000 23:39:30
XMM-Newton		
0090230201	09/03/2001 03:02:28	09/03/2001 09:05:18

et al. (1989). van Paradijs et al. (1988) first observed irregular type I X-ray bursts. Analyzing data of the RXTE satellite, Wijmands et al. (1996, 1998) found a high-frequency quasi-periodic oscillation (QPO) close to 1150 Hz. Subsequently, Ford et al. (1998) found two simultaneous kHz QPOs with a varying frequency separation of about 300 Hz. Hasinger & van der Klis (1989) classified 4U 1735-44 as an atoll source because of its characteristic behavior in a color-color diagram.

The broad-band spectrum of the source was discussed by Seon et al. (1997), who performed a combined analysis of Ginga and ROSAT data. The spectrum was fitted with a combination of a single blackbody and a Comptonization model. Line features were modeled with Gaussian lines. Recently, Lei et al. (2013) analyzed RXTE PCA data with the focus on the timing behavior of the source. The data do not cover the energy range below 2 keV, and compared with *BeppoSAX* and *XMM-Newton* the spectral resolution of the PCA instrument is insufficient for investigating the region of the iron line. Cackett et al. (2009) and Torrejón et al. (2010) found no evidence for an iron line at all based on Chandra observations at a luminosity range of $2.77\text{--}3.37 \times 10^{37} \text{ erg s}^{-1}$. On the other hand, Ng et al. (2010) found a broad iron K_{α} line, with an equivalent width of $43 \pm 13 \text{ eV}$ and a centroid line energy of $6.74 \pm 0.10 \text{ keV}$, investigating an *XMM-Newton* observation taken at a luminosity of $3.98 \times 10^{37} \text{ erg s}^{-1}$.

In this paper, we present for the first time a study of the broad-band spectrum of 4U 1735-44 using data of four *BeppoSAX* observations performed in 2000. We also report on the *XMM-Newton* observation of a broad iron line in the spectrum of the source, investigating the effects of instrumental pile-up on the line shape. We finally suggest a possible source geometry capable of explaining the origin of the observed continuum components and the region where the line formation takes place.

2. Observations

We analyzed data obtained with the X-ray observatories *BeppoSAX* and *XMM-Newton*. The observations are summarized in Table 1. To extract the data products, we followed the corresponding user handbooks of *XMM-Newton*¹ and *BeppoSAX*². The sax tools that were included in the HEASOFT v.5.3³ were used to extract the *BeppoSAX* data. The *XMM-Newton* data products were extracted with the help of the Science Analysis Software (SAS) version 12.0⁴.

BeppoSAX consists of four narrow field instruments, the Low Energy Concentrator Spectrometer (LECS, Parmar et al. 1997), the Medium Energy Concentrator Spectrometer (MECS, Boella et al. 1995), the High Pressure Gas Scintillation Proportional

Counter (HPGSPC, Giarrusso et al. 1995) and the Phoswich Detector System (PDS, Frontera et al. 1995). They allow broad-band X-ray observations in an energy range from 0.2–200 keV, with an effective area of 150 cm^2 at 6 keV (MECS).

Unfortunately, we were unable to use the PDS data in our analysis because of systematic effects above 20 keV. These are due to the location of 4U 1735-44 close to the galactic plane. During the off-pointing of the PDS collimator, the galactic plane fell into the field of view, resulting in an increased number of background-contaminating sources.

The LECS and MECS spectra and lightcurves were used and spectra for the two instruments were extracted from an 8' and 4' region around the source center. The MECS units 2 and 3 were combined and the MECS unit 1 was not used because it developed problems with the voltage supply in 1997.

The four *BeppoSAX* observations have a total exposure time of $\sim 40 \text{ ks}$ for the LECS, $\sim 120 \text{ ks}$ for the MECS and $\sim 82 \text{ ks}$ for the HPGSPC. The LECS and MECS background spectra were extracted from event lists of empty-field observations that are provided by the instrument teams. Since in three of the four observations the collimator of the HPGSPC was not rocking anymore, we summed spectra obtained during Earth occultation to produce a background spectrum, as suggested by the hardware team. This was compared with the off-minus spectrum, the standard background, of the first observation and matched very well. The summed background spectrum provided much better statistics and was therefore used for background subtraction in all four observations.

The observation performed with the EPIC-PN instrument of *XMM-Newton* (Strüder et al. 2001) had an exposure time of 5.3 ks. The EPIC-PN CCD detector is sensitive in the range of 0.1–15 keV and is placed in the focus of an X-ray telescope that offers an effective area of 1500 cm^2 at 6 keV. To cope with the expected high count rate of the source, the EPIC-PN camera was operated in timing mode, which offers a time resolution close to $30 \mu\text{s}$. In timing mode, ten pixels are collapsed to one macropixel, with the spatial resolution limited to one dimension. Despite the relatively high time-resolution of the EPIC-PN camera, pile-up effects had to be properly treated given the high flux of the source. The inner region of the source should be removed from the extraction, if an observation is affected by pile-up, following the suggestion of the hardware team.

To investigate the presence of pile-up we show in Figure 1 and 2 the so-called *epatplot* results obtained with the SAS analysis software. The *epatplot* shows the fractions of the different pattern types compared with those expected from a pile-up free observation. As can be seen in Figure 1, a clear deviation from a pile-up free observation is observed for data extracted within a box with a width of 15 columns (region 1) centered on the source position (column 38). This is indeed expected for a count rate of $\sim 1146 \text{ counts per second}$. In a second step, we excluded the three inner columns (37, 38, and 39) of the box in the extraction. The *epatplot* shown in Figure 2 still showed small deviations from the expected pattern distribution above 10 keV. The resulting count rate of $\sim 470 \text{ counts per second}$ is in the border area in which pile-up effects occur. To compare the effects of pile-up, we also extracted a spectrum without the inner five columns. For this extraction region, there is no evidence for pile-up in the *epatplot*. Finally, we extracted the spectra from four different extraction regions, region 1 with all columns used, region 2 without the innermost column, region 3 without three columns, and region 4 without five columns. To extract the spectra, we used single and double events in an energy range of 0.2–12 keV. The response and the ancillary response file were produced with *rmfgen* and *arfen*, respectively, following the instructions for piled-up ob-

¹ <http://xmm.esac.esa.int/>

² <http://www.asdc.asi.it/bepposax/software/index.html>

³ <http://heasarc.nasa.gov/lheasoft/>

⁴ <http://xmm.esac.esa.int/sas/>

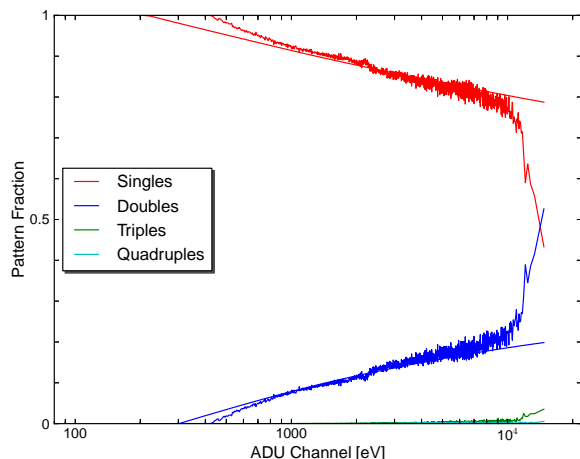


Fig. 1. Epatplot of region 1 (All columns). Shown are the fractions of the different pattern types (singles, doubles, triples, and quadruples). The observed pattern fractions are compared with the expected ones (smooth lines). A deviation is an indication of pile-up. Above 7 keV a clear excess of double events can be seen.

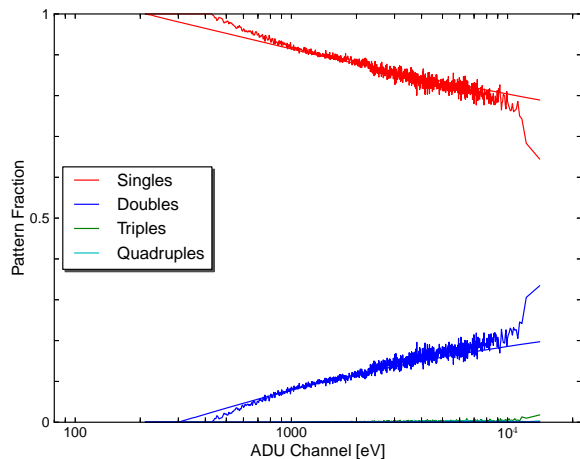


Fig. 2. Epatplot of region 3 (without the innermost three columns). Above 10 keV, an excess of double events is still visible.

servations in the SAS user handbook.

The other two cameras onboard *XMM-Newton* (the MOS cameras, Turner et al. 2001) were both operated in partial window mode, which can handle a source flux of two counts per second. We checked the data for pile-up and found that the observation is piled-up to an extremely high degree, therefore we were unable to use the MOS data in our analysis.

3. Data analysis and observational results

The spectral fittings were all performed using the spectral analysis package XSPEC v.12.7.0 (Arnaud 1996).

3.1. *BeppoSAX*

To study the spectral variation as a function of the source state, we produced a color-color diagram (Figure 3) of all observations, plotting the hard color ($\text{Flux}(7-10\text{ keV})/\text{Flux}(3-7\text{ keV})$) against the soft color ($\text{Flux}(3-7\text{ keV})/\text{Flux}(1-3\text{ keV})$). During

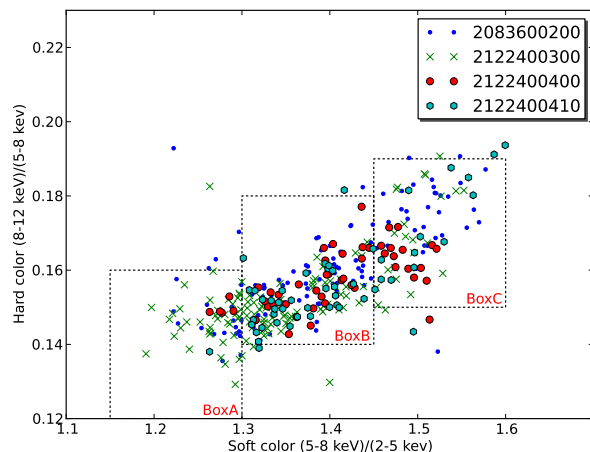


Fig. 3. Color-color diagram for the *BeppoSAX* observation. One point represents 400 seconds of observation. The boxes are discussed at the end of section 3.1.

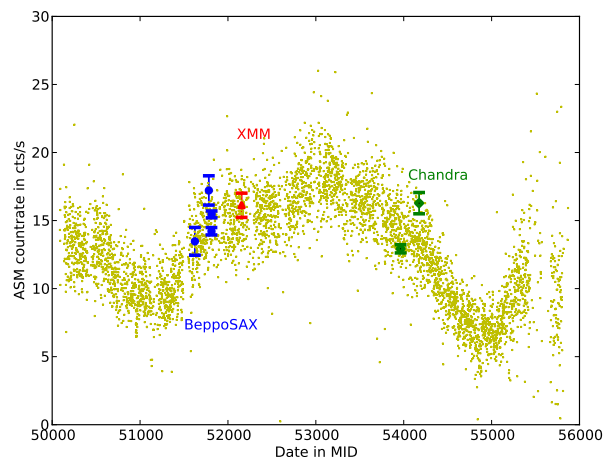


Fig. 4. Whole RXTE ASM light curve. The *BeppoSAX* observations are marked with blue points and the *XMM-Newton* with red triangles. The Chandra observations analyzed by Cackett et al. (2009) are marked with green diamonds to compare the luminosities.

all observations, the source was in the so-called banana state of the atoll sources. To check time variability on timescales shorter than those of the color-color diagram, light curves of the MECS and HPGSPC data were produced. As can be seen in Figure 5, no bursts or dips were found. Although slight changes in the count rate are observed, transitions between different states cannot be unequivocally identified.

To study the intensity of the source on long timescales, the overall light curve of the All Sky Monitor (ASM, Levine et al. 1996) onboard RXTE is plotted in Figure 4. The ASM data indicate that the source was in a similar intensity state during the *BeppoSAX* and the *XMM* observations, in 2000 and 2001 respectively. Furthermore, the Chandra observations, performed in 2006 and 2007, were also taken at a similar ASM intensity and were found to be in the banana state by Cackett et al. (2009). We are therefore confident that all observations were performed when the source was in the banana branch.

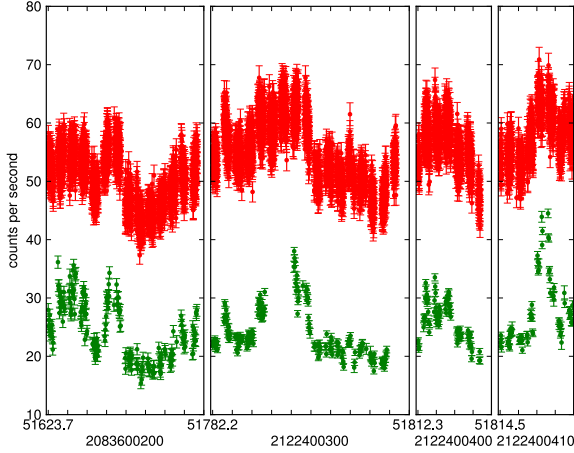


Fig. 5. Light curve of the MECS detector with 16-second time binning (red) and the HPGSPC light curve with a 196-second time binning (green).

For the LECS spectrum, we used the energy bins from 0.2–3.0 keV, for the MECS 1.7–10.0 keV, and for the HPGSPC from 7.0–24.0 keV. Above 24 keV, the HPGSPC data were dominated by the background, so we did not use them. To cope with the uncertainties of the calibration and background subtraction, a systematic error of 2% was applied to the HPGSPC data.

The broad-band continuum was modeled with a photoelectric absorbed (PHABS) combination of a multicolor disk blackbody (DISKBB, Mitsuda et al. 1984) and a thermally Comptonized component (NTHCOMP, Zdziarski et al. 1996; Zycki et al. 1999). The shape of the disk blackbody is determined by the temperature at the inner disk radius T_{in} . Given the source distance, it is possible to calculate the inner disk radius from the normalization defined as $k = (R_{in}[\text{km}]/D[10\text{kpc}])^2 \cos\theta$. The Comptonization component depends on the power-law photon index Γ , the electron temperature kT_e , the seed photon temperature kT_{bb} , and the normalization. Furthermore, the NTHCOMP model allows one to choose between blackbody and disk blackbody seed photons.

The fit of observation 1 resulted in a reduced χ^2 of 2.39 ($\chi^2/\text{DoF} = 409/171$) and some line-like features appeared in the residuals together with an excess above 10 keV. The most prominent feature appeared at energies between 5 and 7 keV, as clearly seen in the middle panel of Figure 6. Since reflection from the accretion disk is observed in LMXBs, we used the REFLIONX model (Ross & Fabian 2005), which models reflection by an optically thick atmosphere, which approximates the surface of an accretion disk well. In fact, the reflection model has recently been used in the analysis of other LMXBs (see Reis et al. 2009; Egron et al. 2011). The spectrum of the reflection depends on the abundance of iron relative to the solar value (Fe/SOLAR). The abundances of the other elements are set to their solar values (Morrison & McCammon 1983). The model also depends on the photon index Γ of the illuminating power-law spectrum, which was fixed in our fits to the Γ of the NTHCOMP because we expect that the illuminating photons originate from regions close to the neutron star. Another free-fit parameter is the ionization, defined as $\xi = 4\pi F/n$, where F is the total illuminating flux and n the hydrogen number density. The best-fit results for the four *BeppoSAX* observations are summarized in Table 2 and the best-fit residuals as well as the unfolded spectrum are shown in Figure 6.

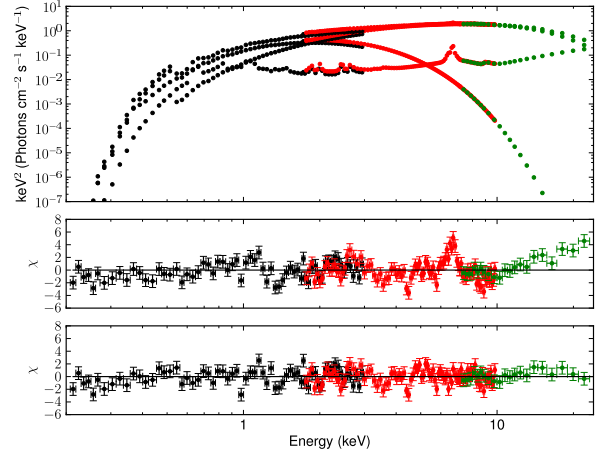


Fig. 6. *BeppoSAX* observation 2083600200 with three instruments: LECS (black), MECS (red), and HPGSPC (green). In the upper panel the unfolded spectra multiplied by E^2 of the best-fit model (PHABS*(DISKBB + NTHCOMP + REFLIONX)) are shown. In the middle panel the residuals above the continuum are plotted, and in the lower panel the residuals after adding the REFLIONX model to the continuum.

Table 2. Best-fit results for the four *BeppoSAX* observations

Parameter	Obs 1	Obs 2	Obs 3	Obs 4
$N_H[10^{22} \text{ cm}^{-2}]$	$0.33^{+0.01}_{-0.02}$	$0.33^{+0.02}_{-0.02}$	$0.30^{+0.01}_{-0.01}$	$0.37^{+0.03}_{-0.03}$
$kT_{dbb}[\text{keV}]$	$0.66^{+0.07}_{-0.16}$	$0.83^{+0.03}_{-0.03}$	$0.76^{+0.07}_{-0.06}$	$0.80^{+0.04}_{-0.03}$
k_{dbb}	432^{+430}_{-115}	251^{+34}_{-28}	288^{+90}_{-70}	291^{+46}_{-49}
Γ	1.62^{fixed}	2.19^{fixed}	1.78^{fixed}	2.31^{fixed}
$kT_e[\text{keV}]$	$2.60^{+0.04}_{-0.04}$	$3.20^{+0.14}_{-0.14}$	$2.80^{+0.06}_{-0.05}$	$3.42^{+0.15}_{-0.15}$
$kT_{bb}[\text{keV}]$	$0.81^{+0.14}_{-0.31}$	$1.34^{+0.04}_{-0.04}$	$1.05^{+0.10}_{-0.04}$	$1.38^{+0.04}_{-0.04}$
$k_{comp}[10^{-2}]$	$13.6^{+6.0}_{-3.6}$	$7.3^{+0.6}_{-0.5}$	$10.2^{+2.0}_{-2.0}$	$7.6^{+0.6}_{-0.6}$
Fe/solar	$1.69^{+0.51}_{-0.43}$	$0.94^{+0.64}_{-0.21}$	$3.23^{+4.78}_{-2.10}$	$1.40^{+1.46}_{-0.57}$
ξ	298^{+132}_{-43}	550^{+139}_{-207}	1996^{+523}_{-730}	559^{+192}_{-198}
$k_{ref}[10^{-6}]$	$13.5^{+5.6}_{-5.5}$	$5.33^{+4.61}_{-2.07}$	$0.94^{+0.87}_{-0.33}$	$7.07^{+3.00}_{-3.25}$
χ^2	212	194	197	193
D.o.f	168	167	167	171
red. χ^2	1.262	1.159	1.179	1.131

For all four observations, statistically meaningful fit results were obtained. All line-like features were properly modeled and the residuals showed no need for an additional model component. We also tried to model the line-like features with Gaussian lines, obtaining higher values of χ^2 and therefore concluding that the REFLIONX model describes the source spectrum better. We also searched for spectral variations along the path of the color-color diagram. Three spectra were obtained by summing the individual spectra of the three boxes defined in Figure 3. The best-fit results slightly changed, but are still within the error range. Hence, no significant spectral variation was detected as a function of the source position in the color-color diagram.

3.2. XMM-Newton

For the nominal energy range of 0.7–10 keV of the EPIC-PN data, the fit showed a broad feature at ~ 1 keV. This feature was found in each of the sources analyzed by Ng et al. (2010). Additionally, features are present in the range of Si and Au absorp-

Table 3. Best-fit results for the four *XMM-Newton* extraction regions. The spectra were extracted from region 1 (all columns), region 2 (without one column), region 3 (without three columns) and region 4 (without five columns). The absorption was frozen to $0.3 \times 10^{22} \text{ cm}^{-2}$.

Parameter	Reg 1	Reg 2	Reg 3	Reg 4
kT_{dbb} [keV]	$1.00^{+0.03}_{-0.03}$	$1.00^{+0.03}_{-0.02}$	$0.98^{+0.04}_{-0.04}$	$0.91^{+0.06}_{-0.05}$
k_{dbb}	147^{+14}_{-16}	157^{+17}_{-16}	172^{+27}_{-25}	211^{+50}_{-45}
kT_{bb} [keV]	$2.04^{+0.03}_{-0.02}$	$2.06^{+0.03}_{-0.03}$	$1.99^{+0.03}_{-0.04}$	$1.85^{+0.04}_{-0.03}$
k_{bb} [10^{-2}]	$5.8^{+0.1}_{-0.1}$	$6.4^{+0.1}_{-0.1}$	$6.3^{+0.1}_{-0.1}$	$5.9^{+0.1}_{-0.2}$
E_{gau} [keV]	$6.79^{+0.09}_{-0.09}$	$6.82^{+0.09}_{-0.09}$	$6.77^{+0.09}_{-0.10}$	$6.70^{+0.15}_{-0.13}$
σ_{gau} [keV]	$0.39^{+0.19}_{-0.13}$	$0.39^{+0.17}_{-0.12}$	$0.37^{+0.12}_{-0.11}$	$0.43^{+0.26}_{-0.17}$
k_{gau} [10^{-3}]	$1.64^{+0.87}_{-0.54}$	$2.01^{+0.93}_{-0.61}$	$2.38^{+1.05}_{-0.76}$	$2.81^{+2.01}_{-1.15}$
EW [eV]	32.4	36.8	43.2	53.2
χ^2	1528	1503	1421	1401
D.o.f	1512	1512	1512	1485
red. χ^2	1.011	0.994	0.94	0.941

tion, which were addressed in an EPIC-PN calibration note⁵. To avoid effects on the fit parameters, we decided to remove the energy bins below 2.4 keV as was done before by e.g. Piraino et al. (2012). In addition, energy bins above 10 keV were not used, as is standard in EPIC-PN observations.

The best fit of the continuum spectral component was achieved by combining an absorbed multicolor disk blackbody `DISKBB` and a single blackbody `WBODY`. Replacing the single blackbody with a Comptonization model, such as `NTHCOMP` or `COMP TT` (Titarchuk 1994), provided an unsatisfactory fit. This is not surprising given the limited energy range of the EPIC-PN data, which leads to problems in constraining the parameters. After modeling of the continuum, line-like residuals are apparent in the energy range of 5–7 keV, as shown in the upper panel of Figure 7 for all four chosen extraction regions. Unfortunately, we could not use the `REFLIONX` model to describe the line features given the limited energy range of the *XMM-Newton* data. This is why we used a simple Gaussian model. The resulting residuals are shown in the middle panel of Figure 7. This model gave acceptable fits with a reduced χ^2 close to 1 for all four regions. Similar statistically acceptable results were also obtained using the model for relativistically broadened iron lines `DISKLINE` (Fabian et al. 1989) (see residuals in the lower panel of Figure 7). Since we obtained similar results with both models, we cannot distinguish a relativistic line profile with respect to a simpler Gaussian broadening. It is worth noting that the radius at which the line is produced is larger than 15 Schwarzschild radii for the `DISKLINE` model. The photoelectric absorption was fixed to $0.30 \times 10^{22} \text{ cm}^{-2}$, the value was obtained with the help of the *BeppoSAX* data since we did not use energy bins below 2.4 keV, which leads to problems in defining the absorption. The best-fit results for the four different extraction regions are summarized in Table 3.

4. Discussion

We have presented the analysis of four broad-band (0.2–24 keV) *BeppoSAX* observations of the LMXB 4U 1735-44. The broad-band spectra were modeled according to the eastern model based on Mitsuda et al. (1984, 1989). The continuum fit suggested the presence of a multicolor disk blackbody, originating from the

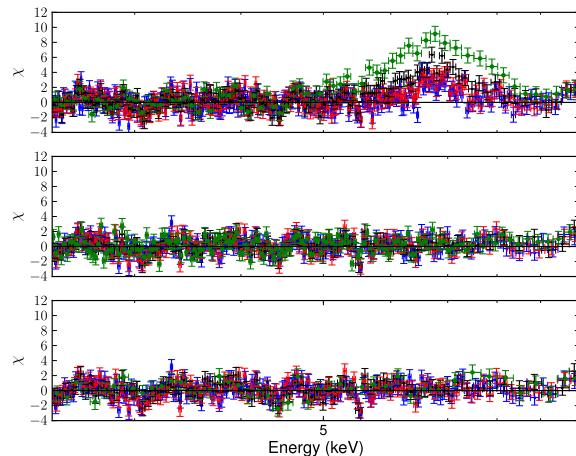


Fig. 7. *Upper panel:* The residuals of all four extraction regions obtained by just using the continuum model. Shown here are region 1 (all columns, blue), region 2 (without one column, red), region 3 (without three columns, black) and region 4 (without five columns, green). *Middle panel:* A Gaussian is added to the continuum model. *Lower panel:* The `DISKLINE` model is used instead of a Gaussian.

disk, and a Comptonized component, most likely due to a corona of hot electrons close to the neutron star in the central region of the accretion disk. From the *BeppoSAX* data, we also concluded that a reflection component can model the residuals of the continuum fit and especially the line-like features well. The most prominent feature was found at 6.7 keV and originates from the iron K_{α} fluorescence line. Although the line is broad, relativistic blurring is not needed to model the line. This indicates that the production site of the observed line is not in the proximity of the neutron star. The inner radius of the accretion can be estimated from the normalization of the `DISKBB` continuum model. We assumed an inclination angle of 60° , which was found as an upper limit by Casares et al. (2006) and is also supported by the absence of dips in the light curve. The hardening factor κ (Shimura & Takahara 1995) was set to 1.7 while the correction for inner boundary conditions was $\xi=0.412$ (Kubota et al. 1998). Eventually, an inner disk radius of 18 to 23 km was estimated from the *BeppoSAX* observations. The inner disk radius is, therefore, between four to six times the Schwarzschild radius for a typical $1.4 M_{\odot}$ neutron star. If we assume a neutron star radius between 10 and 15 km (based on the equation of state summarized in Lattimer & Prakash 2007), this indicates that the accretion disk neither reaches the surface of the compact object nor the innermost stable circular orbit (ISCO), which is three times the Schwarzschild radius. However, if the mass of the neutron star is $2.0 M_{\odot}$, the Schwarzschild radius will be 5.9 km and the 18 km will match the ISCO.

In our analysis of *XMM-Newton* data, we analyzed the line profile, carefully taking into account pile-up and investigating the resulting effects. Ng et al. (2010) claimed that pile-up can produce an asymmetric profile of the iron line. In our analysis, we found no evidence for an asymmetry or broadening of the iron line caused by pile up. On the contrary, we calculated a maximum line width of 0.430 eV (equivalent width of 53.2 eV) after removing the five innermost columns, compared with 0.389 eV (32.4 eV) with all columns. Interestingly, the continuum spectrum became softer when more columns were excluded, which is expected because pile-up hardens the spectrum. The result obtained for the `DISKLINE` model, a production site ra-

⁵ <http://xmm2.esac.esa.int/docs/documents/CAL-TN-0083.pdf>

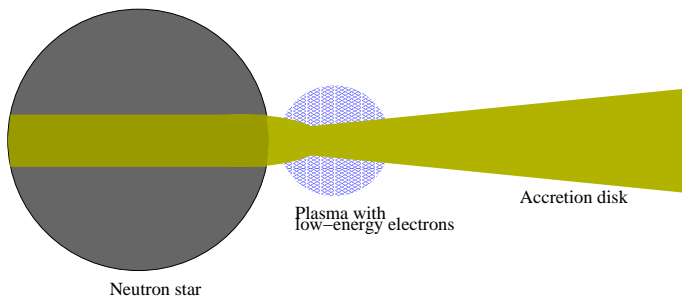


Fig. 8. Possible geometry of the system. Illustration is based on Matsuoka & Asai (2013). A Comptonization region of electrons with an energy of around 3 keV is located close to the neutron star (marked in blue). The accretion takes place at the equatorial regions of the neutron star. The disk emits a multicolor blackbody.

dus of more than 15 Schwarzschild radii (>60 km), confirms that the line production does not take place in the innermost regions of the accretion disk. Moreover the `DISKLINE` model produced an inclination value close to 60° , which supports the assumption used for the *BeppoSAX* data.

According to our results, the model suggested by Sakurai et al. (2012) and Matsuoka & Asai (2013, see Figure 8) might well explain the emission geometry of 4U 1735-44. In the soft state of the source, we observed a Comptonization region of electrons with an average energy of 3 keV located close to the region between the neutron star and the disk. The seed photons are provided by the blackbody, which is emitted at the equatorial region of the neutron star and the inner parts of the accretion disk. Furthermore, we observed a multicolor blackbody spectrum from the disk and the reflection component, which originates from regions of the disk far from the neutron star. The direct emission from the neutron star could not be seen due to the Comptonization region marked blue in Figure 8. Although the model is based on the eastern model, the hot plasma close to the neutron star is similar to the accretion disk corona (ADC) proposed by Church & Balucinska-Church (2004). However, the hot plasma region does not spread as far as the ADC. It remains to be investigated why no line can be found in the analysis of Chandra data. The luminosity was similar to the observations presented in this work and the width of the line exceeded the upper limit given by Cackett et al. (2009, 40 eV).

Acknowledgements. This work is supported by the Bundesministerium für Wirtschaft und Technologie through the Deutsches Zentrum für Luft und Raumfahrt (DLR, grants FKZ 50 OG 1001 and 50 OG 1301). We wish to thank Mrs Sarah Suchy for the careful reading of the manuscript.

References

- Arnaud, K. A. 1996, in *Astronomical Society of the Pacific Conference Series*, Vol. 101, *Astronomical Data Analysis Software and Systems V*, ed. G. H. J. Barnes, 17
- Barr, P., White, N. E., & Page, C. G. 1985, *MNRAS*, 216, 65
- Bhattacharyya, S. & Strohmayer, T. E. 2007, *ApJ*, 664, L103
- Boella, G., Chiappetti, L., Conti, G., et al. 1995, in *Presented at the Society of Photo-Optical Instrumentation Engineers (SPIE) Conference*, Vol. 2517, *Society of Photo-Optical Instrumentation Engineers (SPIE) Conference Series*, ed. S. Fineschi, 223–233
- Cackett, E. M., Miller, J. M., Ballantyne, D. R., et al. 2010, *ApJ*, 720, 205
- Cackett, E. M., Miller, J. M., Bhattacharyya, S., et al. 2008, *ApJ*, 674, 415
- Cackett, E. M., Miller, J. M., Homan, J., et al. 2009, *ApJ*, 690, 1847
- Casares, J., Cornélisse, R., Steeghs, D., et al. 2006, *MNRAS*, 373, 1235
- Church, M. J. & Balucinska-Church, M. 1995, *A&A*, 300, 441
- Church, M. J. & Balucinska-Church, M. 2004, *MNRAS*, 348, 955
- Corbet, R., Smale, A., Charles, P., et al. 1989, *Monthly Notices Of The Royal Astronomical Society*, 239, 533

- D’Ai, A., di Salvo, T., Ballantyne, D., et al. 2010, *A&A*, 516, L36
- di Salvo, T., D’Ai, A., Iaria, R., et al. 2009, *MNRAS*, 398, 2022
- Egron, E., di Salvo, T., Burderi, L., et al. 2011, *A&A*, 530, L99
- Egron, E., Di Salvo, T., Motta, S., et al. 2013, *A&A*, 550, 5
- Fabian, A. C., Iwasawa, K., Reynolds, C. S., & Young, A. J. 2000, *PASP*, 112, 1145
- Fabian, A. C., Rees, M. J., Stella, L., & White, N. E. 1989, *MNRAS*, 238, 729
- Ford, E., Van DER Klis, M., van Paradijs, J., et al. 1998, *Astrophysical Journal*, 508, L155
- Frontera, F., Costa, E., Dal Fiume, D., et al. 1995, in *International Cosmic Ray Conference*, Vol. 2, *International Cosmic Ray Conference*, 41
- Galloway, D., Muno, M., Hartman, J., Psaltis, D., & Chakrabarty, D. 2008, *Astrophysical Journal Supplement Series*, 179, 360
- Giarrusso, S., Santangelo, A. E., Fazio, G., et al. 1995, in *Presented at the Society of Photo-Optical Instrumentation Engineers (SPIE) Conference*, Vol. 2517, *Society of Photo-Optical Instrumentation Engineers (SPIE) Conference Series*, ed. S. Fineschi, 234–248
- Hasinger, G. & van der Klis, M. 1989, *A&A*, 225, 79
- Iaria, R., D’Ai, A., di Salvo, T., et al. 2009, *A&A*, 505, 1143
- Kubota, A., Tanaka, Y., Makishima, K., et al. 1998, *PASJ*, 50, 667
- Lattimer, J. M. & Prakash, M. 2007, *Phys. Rep.*, 442, 109
- Lei, Y. J., Zhang, H. T., Zhang, C. M., et al. 2013, *ArXiv e-prints*
- Levine, A. M., Bradt, H., Cui, W., et al. 1996, *ApJ*, 469, L33
- Matsuoka, M. & Asai, K. 2013, *PASJ*, 65, 26
- Mitsuda, K., Inoue, H., Koyama, K., et al. 1984, *PASJ*, 36, 741
- Mitsuda, K., Inoue, H., Nakamura, N., & Tanaka, Y. 1989, *PASJ*, 41, 97
- Morrison, R. & McCammon, D. 1983, *ApJ*, 270, 119
- Ng, C., Díaz Trigo, M., Cadolle Bel, M., & Migliari, S. 2010, *A&A*, 522, L96
- Pandel, D., Kaaret, P., & Corbel, S. 2008, *ApJ*, 688, 1288
- Parmar, A. N., Martin, D. D. E., Bavdaz, M., et al. 1997, *A&AS*, 122, 309
- Piraino, S., Santangelo, A., & Kaaret, P. 2000, *A&A*, 360, L35
- Piraino, S., Santangelo, A., Kaaret, P., et al. 2012, *A&A*, 542, L27
- Reis, R. C., Fabian, A. C., & Young, A. J. 2009, *MNRAS*, 399, L1
- Ross, R. R. & Fabian, A. C. 2005, *MNRAS*, 358, 211
- Sakurai, S., Yamada, S., Torii, S., et al. 2012, *PASJ*, 64, 72
- Seon, K., Min, K., Yoshida, K., et al. 1997, *Astrophysical Journal*, 479, 398
- Shimura, T. & Takahara, F. 1995, *ApJ*, 445, 780
- Strüder, L., Briel, U., Dennerl, K., et al. 2001, *A&A*, 365, L18
- Tanaka, Y., Nandra, K., Fabian, A. C., et al. 1995, *Nature*, 375, 659
- Titarchuk, L. 1994, *ApJ*, 434, 570
- Torrejón, J. M., Schulz, N. S., Nowak, M. A., & Kallman, T. R. 2010, *ApJ*, 715, 947
- Turner, M. J. L., Abbey, A., Arnaud, M., et al. 2001, *A&A*, 365, L27
- van Paradijs, J., Penninx, W., Lewin, W. H. G., Sztajno, M., & Truemper, J. 1988, *A&A*, 192, 147
- Wijnands, R., van der Klis, M., Mendez, M., et al. 1998, *ApJ*, 495, L39
- Wijnands, R. A. D., van der Klis, M., van Paradijs, J., et al. 1996, *IAU Circ.*, 6447, 1
- Zdziarski, A. A., Johnson, W. N., & Magdziarz, P. 1996, *MNRAS*, 283, 193
- Zycki, P. T., Done, C., & Smith, D. A. 1999, *MNRAS*, 309, 561